Article

Estimation of Aboveground Carbon Stocks in Forests Based on LiDAR and Multispectral Images: A Case Study of Duraer Coniferous Forests

Rina Su [1,2], **Wala Du** [3,4,*], **Hong Ying** [1,2], **Yu Shan** [1,2] and **Yang Liu** [1,2]

[1] College of Geographic Science, Inner Mongolia Normal University, Hohhot 010022, China;
20172104185@mails.imnu.edu.cn (R.S.); hongy864@nenu.edu.cn (H.Y.); yushan@imnu.edu.cn (Y.S.);
20204019011@mails.imnu.edu.cn (Y.L.)

[2] Inner Mongolia Key Laboratory of Remote Sensing and Geographic Information Systems,
Inner Mongolia Normal University, Hohhot 010022, China

[3] Chinese Academy of Agricultural Sciences Grassland Research Institute, Hohhot 010022, China

[4] Arshan Forest and Grassland Disaster Prevention and Mitigation Field Scientific Observation and Research
Station of Inner Mongolia Autonomous Region, Arshan 137400, China

* Correspondence: duwala@caas.cn; Tel.:+86-186-8602-5858

Abstract: The correct estimation of forest aboveground carbon stocks (AGCs) allows for an accurate assessment of the carbon sequestration potential of forest ecosystems, which is important for in-depth studies of the regional ecological environment and global climate change. How to estimate forest AGCs quickly and accurately and realize dynamic monitoring has been a hot topic of research in the forestry field worldwide. LiDAR and remote sensing optical imagery can be used to monitor forest resources, enabling the simultaneous acquisition of forest structural properties and spectral information. A high-density LiDAR-based point cloud cannot only reveal stand-scale forest parameters but can also be used to extract single wood-scale forest parameters. However, there are multiple forest parameter estimation model problems, so it is especially important to choose appropriate variables and models to estimate forest AGCs. In this study, we used a Duraer coniferous forest as the study area and combined LiDAR, multispectral images, and measured data to establish multiple linear regression models and multiple power regression models to estimate forest AGCs. We selected the best model for accuracy evaluation and mapped the spatial distribution of AGC density. We found that (1) the highest accuracy of the multiple multiplicative power regression model was obtained for the estimated AGC (R^2 = 0.903, RMSE = 10.91 Pg) based on the LiDAR-estimated DBH; the predicted AGC values were in the range of 4.1–279.12 kg C. (2) The highest accuracy of the multiple multiplicative power regression model was obtained by combining the normalized vegetation index (NDVI) with the predicted AGC based on the DBH estimated by LiDAR (R^2 = 0.906, RMSE = 10.87 Pg); the predicted AGC values were in the range of 3.93–449.07 kg C. (3) The LiDAR-predicted AGC values and the combined LiDAR and optical image-predicted AGC values agreed with the field AGCs.

Keywords: LiDAR; multispectral images; aboveground carbon stocks; multiple regression model

1. Introduction

With the intensification of global warming and the greenhouse effect, the carbon cycle has become a hot spot in global climate change research [1,2] and forests, as the largest carbon reservoir in terrestrial ecosystems [3] store more than 80% of carbon [4]. Since forest aboveground biomass (AGB) is a key biophysical parameter for measuring carbon and is generally used to quantify the contribution of forests to the global carbon cycle and the forest aboveground carbon stock (AGC) is an important parameter for assessing carbon sequestration capacity and carbon balance above the forest soil layer, it is crucial to understand the role of forests in carbon cycling and climate change.

Forest AGCs have traditionally been measured by field measurements, and although the traditional field measurement method is highly accurate, it is destructive to forests, laborious, and excessively expensive, mainly for small samples [5], and is not suitable for spatially continuous AGC estimation [6]. How to improve the accuracy of spatially continuous forest AGC estimation is still an active research area [7].

Remote sensing can provide accurate and rapid information on vegetation cover over large areas and is now widely used to estimate forest AGB and AGCs [8]. The vegetation indices generated from multispectral images can be used to estimate AGB and AGCs [9]. However, the inability of optical images to penetrate the canopy and provide information on the vertical structure of the forest may lead to uncertain estimates in areas with dense canopies [10,11].

Light detection and ranging (LiDAR) can quickly and accurately acquire 3D information on vegetation [12] and horizontal and vertical structural information on the forest canopy surface and can overcome the optical remote sensing saturation problem, and its emitted laser beam can penetrate the forest canopy. The acquired point cloud can be used to accurately estimate tree height, diameter at breast height, canopy size, and other structural attributes [13,14] and is therefore widely used to estimate AGCs. These LiDAR-derived structural attributes can be used with field measurements to estimate forest AGB through different models. Lu et al. [15] used LiDAR data to extract individual tree structural parameters and input them into an anisotropic growth model to obtain sample-scale AGB. Chen et al. [16] used a multiple regression model to estimate forest AGB and found that the accuracy of the nonlinear model was better than that of the linear model. Luo S et al. [17,18] analyzed the data fusion method of LiDAR and optical images from the perspective of the three-dimensional structure of forest stands, but it is only applicable to data estimation in small areas because of the small coverage area, which limits the utilization of remote sensing data. However, the variables used vary depending on the type of tree species in the study area; determining the best variables remains challenging, and due to the lack of forest canopy spectral information, the accuracy of tree species classification from LiDAR data is limited in complex vegetation conditions [19].

To further improve the accuracy of forest AGB and AGC estimation, a data fusion method of optical images and LiDAR data was proposed [7], which not only provides spectral information but also forest structure information and therefore can improve the accuracy of forest AGC estimation [20,21]. Popescu, S. et al. [22,23] showed that adding a large number of field measurements for modeling based on data fusion can also improve the estimation of forest AGB and AGC. Kim et al. [24] indicated that combining spectral information with attributes derived from LiDAR data is more suitable for assessing AGB and AGC estimates than using optical images or LiDAR data alone. The above study was based on a large amount of field measurement data, and the variables were entered into the regression model to estimate the accuracy. However, there are challenges in finding a method to build a regression model to accurately estimate forest AGCs with relatively few field measurements. We hypothesized that forest-related attributes (tree height, diameter at breast height) combined with remote sensing spectral indices through anisotropic relationships could be used to accurately estimate forest AGCs at the sample plot scale with fewer field measurements.

In this study, we aim to develop a new method for forest AGC estimation by combining forest structural properties and spectral information using the anisotropic relationship assumed above. To improve the estimation of forest AGCs, in this study, we added horizontal structure variables from multispectral images to the measured data and vertical structure variables from LiDAR data to establish a multiple regression model and to explore the effect of combining multisource remote sensing variables on model accuracy. The accuracy was evaluated by comparing and analyzing the multivariate linear model and multivariate power model to estimate the forest AGCs at the sample plot scale. The spatial distribution of AGC density was mapped. This approach enables a more accurate

estimation of forest AGCs and provides data support for the carbon cycle and sustainable forest management.

2. Materials and Methods

2.1. Study Area

The study area (119°28′–120°01′ E, 47°15′–47°35′ N) is located in the middle section of the Daxingan Mountains in the northwestern part of Xing'an League, Inner Mongolia Autonomous Region, and is a comprehensive forestry site integrating natural and planted forests (Figure 1). It borders Mongolia to the west and Hulunbuir to the north and is an essential natural ecological reserve in China. The total area of the forestry field is 4,981,200,000 m^2, of which 334,660,000 m^2 is forestry land, accounting for 67% of the whole area. The forest coverage rate is as high as 61%, and the altitude is mostly 792–1495 m. The region has a cold-temperate continental monsoon climate with an annual average temperature of 1.48 °C; the coldest monthly average temperature is −25.6 °C and the hottest monthly average temperature is 16.6 °C. The mean annual precipitation is 437 mm. The forest is dominated by *Betula platyphylla*, *Larix gmelinii*, and some rare *Populus davidiana* and *Pinus sylvestris*.
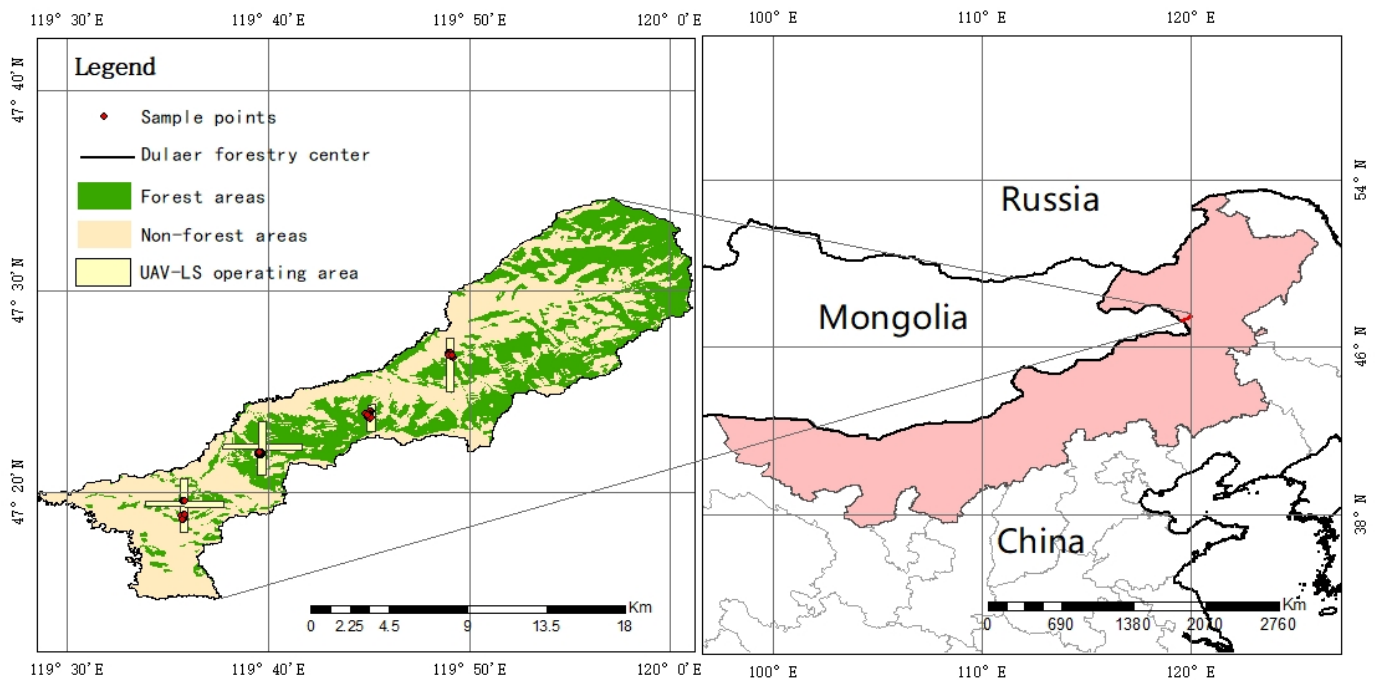

Figure 1. Location of the study area.

2.1.1. Inventory Data

We selected representative sample sites for the field survey in July 2022 based on forest type, slope position, and slope orientation in the area covered by airborne LiDAR data in 2021. We selected 35 natural forest sample sites in the study area according to different tree species and stand densities (Figure 2). Each sample plot was set up as a rectangle of 10 m × 40 m with an area of 400 m^2. The field survey was conducted in July 2022 using a random sampling method to measure the sample plots. A laser rangefinder was used to measure the height of each tree in the sample plot. Trees with a diameter at breast height greater than 0.05 m were selected and measured at a location 1.2 m from the tree using a DBH scale. The coordinates of the centroid and the four corners of the sample were obtained using the differential satellite station technique of the GNSS receiver, which was used to subsequently crop and register the point cloud data.

(**a**)

(**b**)

(**c**)

(**d**)

Figure 2. (**a**) Set up base stations. (**b**) Tree height measurement. (**c**) Obtain the coordinates. (**d**) DBH measurement and record.

2.1.2. Airborne and Ground-based LiDAR

On 15 July 2021, 6 flight strips (5 strips were used for the survey because the steep mountainous terrain made it impossible for people to reach the last strip) were designed with the operating system provided by the long 120 UAV, a long-range six-rotor UAV from CNOOC. The density of the LiDAR point clouds along this flight path was an average of 70 per square meter. The RIEGL VUX-1 LiDAR sensor with the AP15 (X) inertial navigation system acquires LiDAR 3D data with a laser pulse frequency of 600 kHz, a flight altitude of 300 m above ground, and a maximum field of view of 330°.

On 17 July 2022, the LiBackpack DGC50 (Figure 3), a ground-based backpack LiDAR system, was used for the sample site's 3D point cloud data acquisition. Its camera image element is 3840 × 1920, its pixels are 1800 W, the laser's laser wavelength is 9.03×10^{-7} m, and the scanning frequency is 300,000 pts/s. The steps for acquiring point cloud data are as follows: first, a GNSS receiver is used to obtain the absolute coordinates of a point with a stable GPS signal outside the sample area, and a reference station is established at that point to acquire static data. Next, an "S"-shaped route is designed, and the surveyor connects the phone to the LiBackpack to see the number of satellites searched and view the point cloud on the phone while collecting data in real-time. Data are collected while walking during

the LiBackpack data acquisition process to avoid obstructions and to ensure high-quality point cloud data.

Figure 3. LiBackpack DGC50 LiDAR scanning system.

2.1.3. Multispectral Imaging

On 11 July 2021, the Pegasus V300 UAV with the D-CAM2000 sensor acquired multispectral data for six sample bands, i.e., the blue, green, red, red-edge, near-infrared, and panchromatic bands (see Table 1). The flight operation design altitude was 383 m, the heading overlap rate was 80%, the side overlap rate was 60%, and the sensor was equipped with an IMU inertial navigation system to ensure a spatial resolution of 0.02 m.

Table 1. Multispectral image band parameters.

Band	Band Name	Wavelength	Wave Width	Spatial Resolution (m)
Band 1	Visible Blue Light	475	20	0.2
Band 2	Visible Green Light	560	20	0.2
Band 3	Visible Red Light	668	10	0.2
Band 4	Red	840	40	0.2
Band 5	NIR	717	10	0.2
Band 6	Panchromatic Band	-	-	-

2.2. Data Processing Approach

Ground-based forestry preprocessing, such as denoising, ground point classification, data elevation model (DEM) generation, normalization, and single wood segmentation was performed on LiDAR point cloud data, and variables such as tree location, tree height, DBH, crown diameter, crown area, and crown volume were obtained from the single wood segmentation. Five vegetation indices, including the normalized difference vegetation index (NDVI), ratio vegetation index (RVI), enhanced vegetation index (EVI), difference vegetation index (DVI), and adjusted soil brightness vegetation index (SAVI), were calculated after preprocessing the multispectral images with cropping, atmospheric correction, radiometric calibration, and band synthesis. The point cloud data and multispectral image data are then filtered for variables. The measured AGC was the dependent variable, and

the LiDAR structural attributes (tree height, DBH) were used as independent variables for linear and nonlinear modeling to estimate the LiDAR AGC. Similarly, the measured AGC was used as the dependent variable. The multispectral index (NDVI), diameter at breast height based on LiDAR data, and tree height were used as independent variables for linear and nonlinear multisource remote sensing AGC estimation modeling. The optimal model was selected to verify the accuracy and produce a spatial distribution of the AGC density. The technical route is shown in Figure 4.
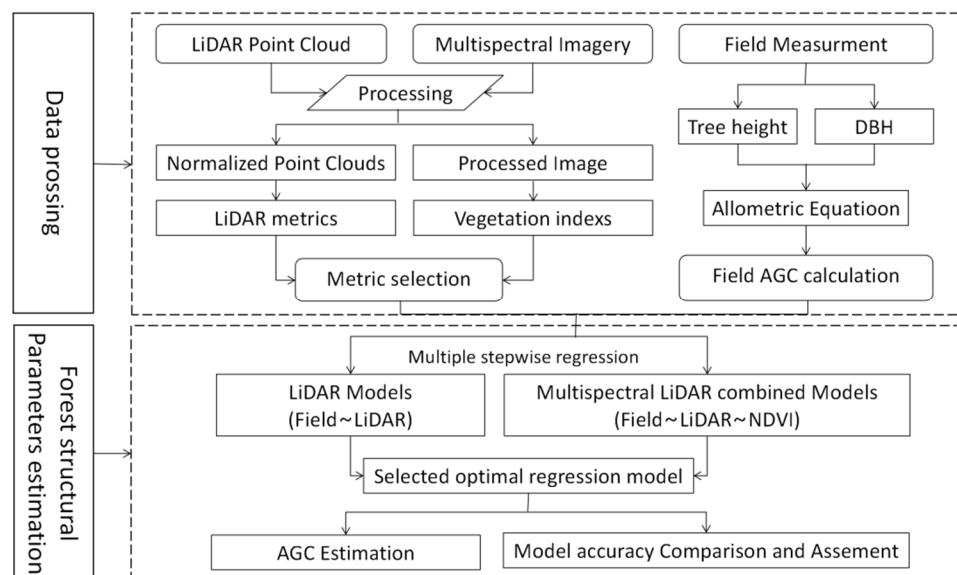

Figure 4. Data processing workflow.

2.2.1. Field Inventory

The anisotropic growth equation is the basis for calculating the biomass of tree organs and vegetation carbon stocks and for estimating the rate and potential of carbon sequestration by trees [25]. Currently, most forest biomass estimation studies are based on the selection of existing allometric growth equations or allometric growth equations fitted from resolved wood data according to the study area [26]. In this study, we estimated the AGC of *L. gmelinii* in the Dural forest based on the allometric growth equation [27] of dominant tree species in Inner Mongolian forests (Table 2). The total AGB of the forest in the study area is shown in Equation (1).

$$AGB = B_{Stem} + B_{Branch} + B_{Leaf} + B_{Bark} \tag{1}$$

where AGB is the total aboveground biomass; B_{Stem} is the trunk biomass; B_{Branch} is the branch biomass; B_{Leaf} is the leaf biomass; B_{Bark} is the bark biomass.

Table 2. Allometric growth equations of Inner Mongolian *L. gmelinii*.

Organ	Allometric Growth Equation of *L. gmelinii*	Reference
Stem	$B_{Stem} = 0.0437 \, (D^2H)^{0.9781}$	[27]
Branch	$B_{Branch} = 0.8813 \, (D^2H)^{0.2237}$	[27]
Leaf	$B_{Leaf} = 0.0317 \, (D^2H)^{0.4017}$	[27]
Bark	$B_{Bark} = 0.0593 \, (D^2H)^{0.4197}$	[27]

D denotes tree diameter at breast height; H denotes tree height; B_{Stem} denotes tree trunk biomass; B_{Branch} denotes branch biomass; B_{Leaf} denotes leaf biomass; and B_{Bark} denotes bark biomass.

In this study, aboveground biomass was converted to carbon stock using the default value of 0.5 provided by the IPCC [28], as shown in Equation (2).

$$AGC = 0.5 \times AGB \tag{2}$$

where AGC is the entire aboveground carbon stock.

The final measured AGC was obtained by simplifying Equations (1) and (2), as shown in Equation (3).

$$AGC_{measured} = 0.0407 \times (D^2H)^{0.9083} \tag{3}$$

where D is the diameter at breast height and H is the tree height.

To verify the feasibility of estimating forest AGC based on LiDAR and multisource data, measured data and estimates were used as reference values. The coefficient of determination (R^2) and root mean square error (RMSE) were used to assess the model's accuracy. The calculation equations are as follows.

$$R^2 = 1 - \frac{\sum_{i=1}^{n}(y^i - \hat{y}_i)^2}{\sum_{i=1}^{n}(y^i - \overline{y}_i)^2} \tag{4}$$

$$RMSE = \sqrt{\frac{\sum_{i=1}^{n}(\hat{y}_i - y_i)^2}{n}} \tag{5}$$

where n is the number of samples; y^i and $\hat{y}_i$ are the respective measured AGC and estimated AGC of the ith sample; and $\overline{y}_i$ is the average AGC of the ith sample.

The summary statistics of the forest parameters obtained from the field measurements are presented in Table 3.

Table 3. Summary statistics of the field-measured forest parameters.

Parameter	Min.	Max.	Mean	Std.
H (m)	3.20	15.5	9.71	2.74
DBH (m)	0.06	0.35	0.15	4.24
AGC (kg C)	2.59	285.48	51.13	37.31

2.2.2. LiDAR

LiDAR data were processed using Insta360studio, LiFuser BP, and LiDAR360. Colors were attached to the collected sample plots with Insta360studio. The data SLAM-solving work was performed with LiFuser BP, and LiDAR360 was used to extract the structural attributes of the trees. First, the original point cloud data and trajectory files and GNSS static data were imported into LiFUser BP software for trajectory solving to obtain the point cloud data that contained the absolute geographic location information. Next, the solved LiBackpack data were imported into LiDAR360 for processing; the point cloud data were cropped according to the sample range and filtered after redundancy and noise removal, and then the ground points were classified. Finally, irregular triangular grid interpolation was used to generate a digital elevation model (DEM). The point cloud was normalized based on the DEM to eliminate the influence of topography on tree height estimation. Figure 5 shows the collected sample plots based on elevation and RGB.
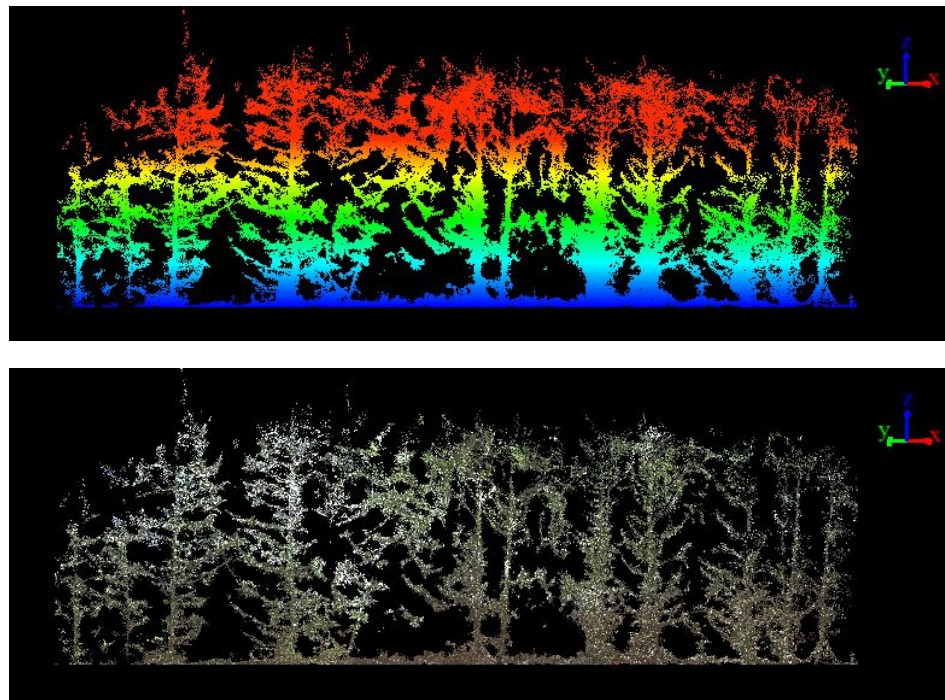
Figure 5. Backpack LiDAR data acquisition and point cloud data.

2.2.3. Multispectral Image Processing

The forest spectral information on remote sensing images mainly comes from the degree of reflection, absorption, and scattering of the solar spectrum by the forest canopy, and the chlorophyll content of forest vegetation leaves is an important indicator of photosynthetic capacity and the degree of dry matter accumulation. The spectral difference between infrared and near-infrared bands of plants can reflect the chlorophyll content and dry matter accumulation of vegetation, i.e., the biomass of forest vegetation can be calculated from the spectral information of forest vegetation. The spectral information in different bands can reflect the growth status and biomass of different vegetation. Therefore, some vegetation indices obtained by analytical operations in the spectral band can provide better vegetation growth and biomass. In this study, the UAV remote sensing multispectral image map of the test area was first preprocessed with cropping, atmospheric correction, and radiometric calibration. Then, five vegetation indices, i.e., the normalized vegetation index (NDVI), ratio vegetation index (RVI), enhanced vegetation index (EVI), differential vegetation index (DVI), and adjusted soil brightness vegetation index (SAVI), were calculated separately (Table 4).

Table 4. Vegetation indices calculation.

Variable	Equation	Description	Reference
R, G, B, NIR	B1, B2, B3, B4	Bands	-
NDVI	$(B4 - B3)/(B4 + B3)$	Normalized difference vegetation index	[29]
RVI	$B4/B3$	Ratio vegetation index	[30]
EVI2	$2.5 \times (B4 - B3)/(B4 + 2.4 \times B3 + 1)$	Enhanced vegetation index2	[31]
DVI	$B4 - B3$	Difference vegetation index	[32]
SAVI	$1.5 \times (B4 - B3)/(B4 + B3 + 0.5)$	Soil-adjusted vegetation index	[33]

3. Results

3.1. Estimation of the AGC Based on LiDAR

The modeling method used a simple regression fitting method to model the LiDAR-estimated tree height and diameter at breast height with the forest AGC. The model

accuracy was evaluated using R^2 and RMSE. Among the various methods currently used to invert the aboveground biomass of vegetation based on remote sensing information, the multiple linear regression method is suitable for the regional scale. It has a high estimation accuracy [34]. In this study, models were fitted to forest structure variables such as DBH and tree height with the predicted AGC, and the best-fit model was selected from multiple models (Table 5).

Table 5. LiDAR-predicted AGC modeling regression analysis.

Argument	Model	R^2	RMSE
DBH_{LiDAR}	$AGC_{LiDAR} = 0.0661 \times DBH_{LiDAR}{}^{2.3896}$	0.903	10.91
DBH_{LiDAR}	$AGC_{LiDAR} = 8.1288 \times DBH_{LiDAR} - 72.68$	0.853	14.29
H_{LiDAR}	$AGC_{LiDAR} = 6.3525 \times H_{LiDAR}{}^{0.8541}$	0.192	34.13
H_{LiDAR}	$AGC_{LiDAR} = 5.6161 \times H_{LiDAR} - 0.9979$	0.244	32.44
$DBH_{LiDAR} \times H_{LiDAR}$	$AGC_{LiDAR} = 0.1999 (DBH_{LiDAR} \times H_{LiDAR})^{1.0948}$	0.660	19.29
$DBH_{LiDAR} \times H_{LiDAR}$	$AGC_{LiDAR} = 0.4076 (DBH_{LiDAR} \times H_{LiDAR}) - 8.5008$	0.746	18.82
$DBH_{LiDAR} + H_{LiDAR}$	$AGC_{LiDAR} = 0.013 (DBH_{LiDAR} + H_{LiDAR})^{2.5381}$	0.796	13.44
$DBH_{LiDAR} + H_{LiDAR}$	$AGC_{LiDAR} = 5.3492 (DBH_{LiDAR} + H_{LiDAR}) - 79.995$	0.794	16.94

Table 5 shows that among all of the multivariate linear models and multivariate power models, the multivariate power model was more accurate than the multivariate linear model. The LiDAR-estimated tree height (power function) had the lowest AGC fit (R^2 = 0.192, RMSE = 34.13). The DBH (power function) estimated by LiDAR was the best fit for the predicted AGC (R^2 = 0.903, RMSE = 10.91). The combined LiDAR-estimated diameter at breast height and tree height significantly improved the predicted AGC fit over the calculated tree height alone. The coefficient of determination (R^2) improved from 0.192 to 0.794. However, it was lower than that based on the diameter at breast height alone. Therefore, we used a simple power function regression model with the LiDAR-estimated diameter at breast height as a predictor to simulate the predicted AGC, and the predictive regression model is shown in Equation (6).

$$AGC_{LiDAR} = 0.0661 \times DBH_{LiDAR}{}^{2.3896} \tag{6}$$

As shown in Figure 6, the LiDAR-predicted AGC was significantly correlated with the measured AGC. The R^2 of the LiDAR inversion-predicted AGC was 0.903, and the RMSE was 10.92.
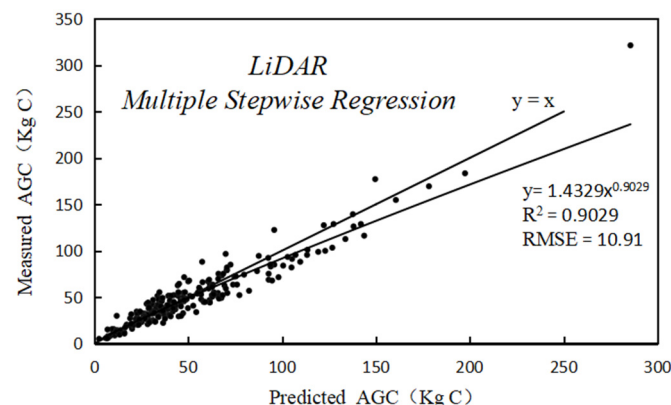

Figure 6. Correlation between the LiDAR-predicted AGC and the measured AGC.

Based on the AGC density values from the LiDAR estimation model, the spatial distribution of the AGC density at the sample scale was plotted in ArcGIS by inverse distance weight interpolation, as shown in Figure 7. The minimum AGC predicted by LiDAR was 4 kg C, and the maximum AGC was 280 kg C. These values are consistent with the measured AGC of 2.6–285 kg C (Table 3).
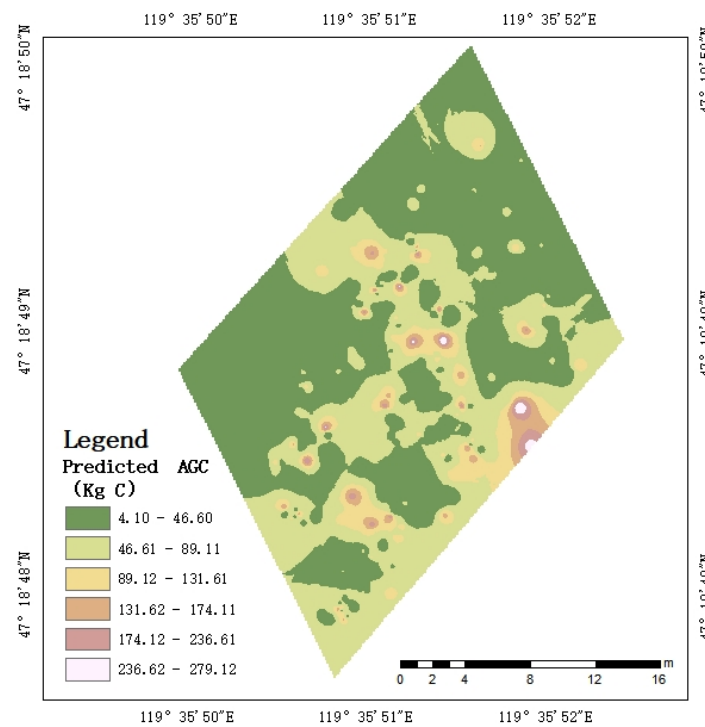
Figure 7. LiDAR-predicted AGC spatial distribution map.

3.2. Estimation of the AGC Based on Combined LiDAR and Multispectral Images

LiDAR data have shortcomings, i.e., they are spatially discrete and do not have imaging capability; therefore, the estimation of forest AGC was achieved by combining multispectral information based on LiDAR-obtained tree height and diameter at breast height. The vegetation indices based on spectral information combined with LiDAR inversion vegetation parameters for modeling estimation can improve the fit and inversion accuracy of AGC estimation [35]. In this study, based on the previous estimation of forest AGC using LiDAR data, the inversion model was optimized by combining multispectral images to complement the vegetation spectral information. The results of the Pearson correlation analysis between the five vegetation indices and the measured AGC using the statistical analysis software SPSS are shown in Table 6. The five selected vegetation indices were positively correlated with the measured AGC. NDVI was significantly positively correlated with the measured AGC at the 0.01 level with a correlation coefficient of 0.236. Correlation analysis was performed to screen the optimal vegetation indices, which improved the accuracy of the estimated AGC. This reduces unnecessary computational processes and brings convenience to biomass inversion modeling. This approach can also effectively replace the whole vegetation index study, reduce the survey elements, simplify the relationship between indicators, and make the model calculation more representative.

Table 6. Correlation between vegetation indices and measured AGC.

Vegetation Index	Correlation
NDVI	0.236 **
RVI	0.095
EVI2	0.093
DVI	0.123
SAVI	0.094

** indicates a significant correlation at the 0.01 level (double-tailed).

This study combined the multispectral index (NDVI) with LiDAR data to model biomass using multiple linear and nonlinear equations. The optimal model was selected

from the various models to predict the AGC. As seen in Table 7, the multivariate power model was more accurate than the multivariate linear model as the regression model for predicting the AGC from LiDAR data. The prediction of the AGC using NDVI alone was poor (R^2 = 0.056, RMSE = 36.25), and the addition of LiDAR parameters (diameter at breast height and tree height) significantly increased the AGC prediction with significantly better modeling accuracy. The highest accuracy (R^2 = 0.906, RMSE = 10.87) was obtained for the AGC model with a simple power function fit of NDVI combined with LiDAR diameter at breast height prediction; the accuracy was higher than that obtained using only LiDAR data (Table 5). This result precisely reflects that although the vegetation index can reflect certain information on the horizontal structure of vegetation cover, it lacks information on the vertical form of vegetation height and is prone to saturation. However, the inclusion of LiDAR parameters overcame the saturation problem and improved the estimation accuracy of the AGC.

Table 7. Regression analysis of NDVI combined with LiDAR parameters to predict biomass.

Argument	Models	R^2	RMSE
NDVI	$AGC_{NDVI} = 105 \times NDVI - 22.04$	0.056	36.25
NDVI + H_{LiDAR}	$AGC_{NDVI+H(LiDAR)} = 5.5279 \times (NDVI + H_{LiDAR}) - 4.0316$	0.243	32.45
NDVI $\times$ H_{LiDAR}	$AGC_{NDVI \times H(LiDAR)} = 6.4484 \times (NDVI \times H_{LiDAR}) + 8.4591$	0.238	32.56
NDVI + DBH_{LiDAR}	$AGC_{NDVI+DBH(LiDAR)} = 8.1248 \times (NDVI + DBH_{LiDAR}) - 78.281$	0.857	14.11
NDVI + DBH_{LiDAR}	$AGC_{NDVI+DBH(LiDAR)} = 0.0419 \times (NDVI + DBH_{LiDAR})^{2.5139}$	0.906	10.87
NDVI $\times$ DBH_{LiDAR}	$AGC_{NDVI \times DBH(LiDAR)} = 9.7909 \times (NDVI \times DBH_{LiDAR}) - 53.242$	0.830	15.37
NDVI $\times$ DBH_{LiDAR}	$AGC_{NDVI \times DBH(LiDAR)} = 0.8306 (NDVI \times DBH_{LiDAR})^{2.014}$	0.826	12.81

This study used a simple power function regression model to simulate the AGC using the NDVI combined with LiDAR inversion of the diameter at breast height as a predictor. The expected regression model is shown in Equation (7).

$$AGC_{NDVI+DBH_{LiDAR}} = 0.0419 \times (NDVI + DBH_{LiDAR})^{2.5139} \tag{7}$$

The AGC predicted by multispectral information combined with LiDAR data was obtained using Equation (7). As shown in Figure 8, the AGC predicted using the multispectral information combined with LiDAR data correlated significantly with the measured AGC. The predicted R^2 for AGC was 0.906, and the RMSE was 10.87.
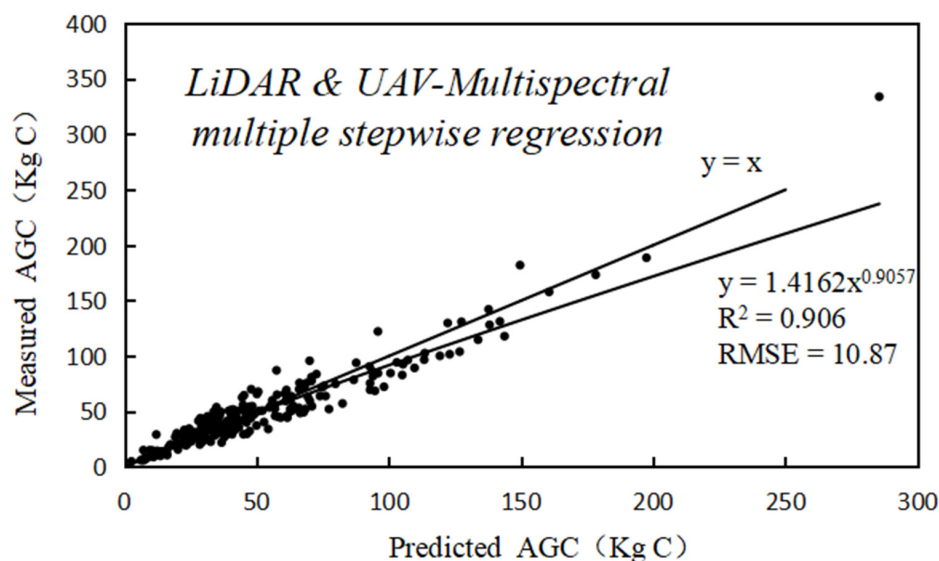

Figure 8. Multispectral information combined with LiDAR data was used to predict the AGC. Correlation between the predicted and measured AGC.

The spatial distribution of AGC density by inverse distance weight interpolation in ArcGIS, combining the estimated model AGC density values from LiDAR and multispectral data, is shown in Figure 9. The minimum AGC predicted by the multisource data was 3.93 kg C, and the maximum AGC was 449 kg C, which is higher than the measured AGC and the AGC predicted by LiDAR.
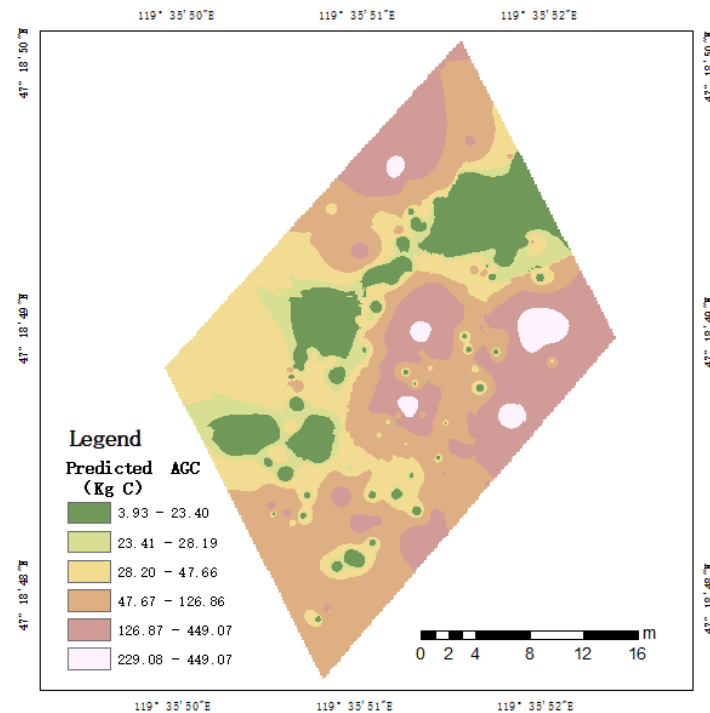

Figure 9. Predicted AGC spatial distribution map based on a combination of LiDAR and multispectral data.

4. Discussion

4.1. Potential of LiDAR and Multispectral Image Synergy for Forest AGC Estimation

Compared to manual surveying, the backpack LiDAR allows for accurate scanning and real-time data integration while on the move, providing a more flexible and efficient way to collect data for forest inventory [36]. The backpack LiDAR requires only one surveyor to carry the equipment across the survey site during data acquisition, significantly reducing time and costs and increasing efficiency [37]. As shown in Table 8, when collecting point cloud data of 10 m × 40 m samples, the traditional measurement method requires 3–4 people to collect the data at the same time, while the backpack LiDAR only requires 1 person to complete the collection; the traditional manual measurement takes approximately 36 min to finish measuring a sample area, while the backpack LiDAR only takes approximately 5 min; the traditional measurement method requires preprocessing of the collected data (inputting the data on the record sheet into Excel), which takes approximately 14 min, while the backpack LiDAR takes approximately 10 min to preprocess the data. The time required for preprocessing the collected data (inputting the data on the record sheet into Excel) is approximately 14 min, while the preprocessing time for the backpack LiDAR point cloud data is approximately 10 min, and the internal data processing time depends on the size of the data set and the computer configuration; overall, the time spent by the backpack LiDAR after collecting a sample plot is approximately 30 min faster than the traditional measurement method. The above description illustrates the time efficiency of backpack LiDAR. For optical data, acquiring airborne multispectral images in good weather conditions improves efficiency and reduces costs to some extent. Thus, the use of combined optical imagery and LiDAR further reduces the cost of assessing forest abatement. It makes it possible to map near real-time carbon stocks over large areas [38].

Table 8. Timing comparison between traditional and backpack LiDAR measurement methods.

Measurement Method	Personnel	Sample Site (m^2)	Time Consumption (min)		
			Data Collection	Data Processing	Total
Traditional measurement	3–4	10 × 40	30:16	14:16	44:32
Backpack LiDAR	1	10 × 40	5:42	10:04	15:46

Optical images have been applied in earlier studies to estimate forest AGB and AGC, but the results show that the penetration of optical signals is weak. Spectral images mainly record the horizontal structure of the forest and cannot record the vertical structure information of the woods. However, LiDAR can penetrate the forest canopy and record the vertical structure information. It is good to make up for the deficiency of optical images. In this study, there are two main reasons why the improvement with the addition of multispectral information is slight. The first reason could be that when visible light from multispectral data is saturated in dense forest areas [39], the accuracy is lower in complex forest structures, resulting in deviations between the estimated and measured AGC of NDVI. Another reason could be that LiDAR forest structure properties are strongly correlated with AGC, and adding multispectral information does not improve much. Although these improvements are not significant, the novel multisensor earth observation approach combining satellite-based LiDAR data using machine learning techniques for optical data has enabled accurate measurements of carbon stocks and provided adequate data support for forest mitigation [40–43]. For example, Jiao et al. [38] proposed a practical framework for assessing forest abatement using the fusion of optical satellite images and spaceborne LiDAR data. Shen et al. combined Landsat TM/ETM + and ALOS l-band SAR images of Guangdong Province to map AGB data of subtropical forests. The results showed a good correlation of AGB based on multisensor photos [44]. Our results further suggest that combining LiDAR data and multispectral data is essential to improve the accuracy of AGB and AGC estimation.

4.2. Analysis of the Major Challenges and Uncertainties in Estimating Forest AGC

To address the challenges in vegetation biomass and carbon stock estimation (i.e., whether the simultaneous acquisition of large-scale forest structural and spectral information can improve the analysis of biomass and carbon stocks [14,45]), in this study, we combined forest structural attributes and spectral data to estimate forest AGC at the sample plot scale. (1) Although it is difficult to accurately capture changes in forest AGCs using only structural and spectral information for forest stands with complex structures, our proposed combined modeling approach with multisource data improved the accuracy of AGC estimation from 90.29% to 90.6% because the information on canopy spectral heterogeneity was provided by multispectral images. (2) In addition, we selected the best regression model to fit the AGC from multiple linear regression models and multiple power regression models. Multiple power regression models had higher AGC estimation accuracy than multiple linear regression models (Tables 5 and 7). This suggests that the *L. gmelinii* in our study area is consistent with a power anisotropy relationship. The use of the power anisotropic relationship can improve the accuracy of forest AGC estimation, and this relationship based on forest structural properties and spectral information is a new approach to improving forest AGC estimation. Based on forest structural attributes and spectral information, this method can be used to explore the relationship between tree metabolism and biomass [46], and this relationship may be more stable in similar landscapes [7].

There are still some uncertainties in this study. First, the backpack LiDAR laser beam cannot penetrate the lower canopy in dense forest structures [47]. Second, the backpack LiDAR has challenges capturing the tops of trees in the upper canopy due to the shading caused by trees in the lower canopy, thus leading to significant differences between the height estimated by LiDAR and the measured height in this study. All the experimental

results and conclusions of this study are currently valid only for coniferous forests with relatively simple stand structures, and their validity in broadleaf forests, mixed forests, or other forest types with more complex stand structures needs to be verified based on more forest sample plots and remote sensing data.

4.3. Estimating the Late Stage of Forest AGC Research and Outlook

This study focuses on the theme of combining multispectral images and LiDAR data for estimating regional-scale forest AGC, from field sample measurements to preprocessing such as atmospheric correction, radiometric correction, and geometric correction of multi-spectral images and LiDAR data cropping, resampling, denoising, filtering, near-ground classification, and normalized point clouds, to constructing a forest AGC estimation model for complex terrain conditions and then performing spatial extension of forest AGC at the regional scale. However, due to the shortage of measured data and the complexity of mountainous terrain conditions, the accuracy of regional forest AGC estimation by combining multisource remote sensing data is not currently accurate. A series of studies need to be continued.

At the current stage, calibration and validation still require high-quality field real-world data. Due to the complexity of mountainous terrain conditions, more accessible locations were selected to collect field inventories, leading to spatial discontinuity and discrete problems in producing regional forest AGC density spatial distribution maps. In future studies, we will try to select spatially continuous sample sites to collect data. Due to time constraints, limited samples were collected, and more minor sample data were only applicable to single wood or regional forest AGC estimation. It could not represent the forest AGC stock in the whole Dural Forest.

Poor GPS signals during data acquisition by backpack LiDAR can directly affect the quality of the track files, leading to point cloud solution failure or point cloud data solution failure with significant absolute coordinate errors. In addition, acquiring point cloud data with high-precision absolute coordinates is crucial for localizing individual trees in the sample area. Therefore, how to efficiently and accurately acquire absolute georeferenced point cloud data in a dense forest without GPS signals by backpack LiDAR is the focus of future research. In addition, the *L. gmelinii*-like ground has dense branches. To avoid scratching the backpack LiDAR instrument, the branches must be cut off in advance along the design route to ensure the safe operation of the backpack LiDAR. Therefore, the timing and quality of backpack LiDAR data acquisition due to forest stands and the accuracy of image data acquisition need to be further verified in more operating environments. Due to the small amount of spectral band data acquired from the multispectral data used in this study, the calculated vegetation spectral indices correlate less with the forest AGC. In future studies, the ability of UAVs with hyperspectral imagers at different flight altitudes to acquire regional forest vegetation spectra and combine them with LiDAR data for regional forest carbon stock inversion needs to be explored.

In general, the combination of LiDAR data and traditional remote sensing data can better complement each other's data sources, which will help the acquisition and classification of feature information, improve the accuracy of estimating various parameters of ecosystems, and enhance the overall function of ecological monitoring and simulation. How to effectively combine multiple remote sensing data sources for environmental research is a hot issue.

5. Conclusions

In this study, based on the measured data, LiDAR vertical structure variables, and the addition of multispectral image horizontal structure variables to establish a multiple regression model, the following conclusions were obtained by comparing and analyzing the multivariate linear model and the multivariate power model to estimate the forest AGC at the sample scale.

A multivariate model was developed to predict the AGC and was tested for accuracy using LiDAR-estimated DBH and tree height as independent variables and the measured AGC as the dependent variable. The highest accuracy of the estimated AGC was found for the multiplicative power regression model based on LiDAR-estimated DBH (R^2 = 0.903, RMSE = 10.91 Pg). The AGC values predicted by LiDAR ranged from 4.1–279.12 kg C. The accuracy of the LiDAR-estimated diameter at breast diameter was much higher than that of the tree height. This result may be due to the tall vegetation cover in the study area and the narrow beam of ground-based LiDAR, which makes it very difficult to search for targets in space due to the influence of occlusions and directly affects the interception probability and detection efficiency of the targets.

LiDAR data combined with the multispectral estimation of the AGC and determination of the accuracy showed that the multiplicative power regression model with the highest accuracy included the DBH-predicted AGC estimated by NDVI combined with LiDAR data (R^2 = 0.906, RMSE = 10.87 Pg); the predicted AGC values were in the range of 3.93–449.07 kg C. The accuracy of AGC inversion using NDVI alone was extremely low (R^2 = 0.056, RMSE = 36.25). This is because multispectral optical image data cannot accurately reflect vegetation height information, and spatial data effects are lacking.

Multiple regression analysis modeling demonstrated the potential of estimating the AGC from multisource remote sensing data. The model's prediction accuracy was high (R^2 = 0.87–0.90) compared to the prediction accuracy in other studies [48,49]. The results showed that the addition of multispectral image variables to the predictive model for LiDAR estimation explained the variation in AGC estimation improvement. When LiDAR data and multispectral data are combined to estimate the AGC, LiDAR data are both accurate and include the spectral characteristics of multispectral optical images.

In general, the AGC is related not only to the structural features of trees that can be extracted from LiDAR data but also to the carbon coefficients that can be reflected in the multispectral information. Therefore, if both LiDAR and multispectral data are available, the fusion of LiDAR with multispectral data is the best method to accurately estimate forest AGC. This study could provide a valuable resource for researchers and forest managers to obtain more accurate AGC values.

References

1. Cook-Patton, S.C.; Leavitt, S.M.; Gibbs, D.; Harris, N.L.; Lister, K.; Anderson-Teixeira, K.J.; Briggs, R.D.; Chazdon, R.L.; Crowther, T.W.; Ellis, P.W.; et al. Mapping Carbon Accumulation Potential from Global Natural Forest Regrowth. *Nature* **2020**, *585*, 545–550. [CrossRef] [PubMed]
2. Mitchard, E.T.A. The Tropical Forest Carbon Cycle and Climate Change. *Nature* **2018**, *559*, 527–534. [CrossRef] [PubMed]
3. Lorenz, K.; Lal, R. *Carbon Sequestration in Forest Ecosystems*; Springer: Dordrecht, The Netherlands, 2010; p. 279. [CrossRef]
4. Waring, R.H.; Running, S.W. Forest Ecosystems: Analysis at Multiple Scales. *Choice Rev. Online* **1998**, *36*, 36–1577. [CrossRef]
5. Mutanga, O.; Shoko, C.; Adelabu, S.; Bangira, T. Remote Sensing of Aboveground Forest Biomass: A Review. *Trop. Ecol.* **2016**, *57*, 125–132.
6. Viana, H.; Aranha, J.; Lopes, D.; Cohen, W.B. Estimation of Crown Biomass of Pinus Pinaster Stands and Shrubland Above-Ground Biomass Using Forest Inventory Data, Remotely Sensed Imagery and Spatial Prediction Models. *Ecol. Model.* **2012**, *226*, 22–35. [CrossRef]
7. Yang, Q.; Su, Y.; Hu, T.; Jin, S.; Liu, X.; Niu, C.; Liu, Z.; Kelly, M.; Wei, J.; Guo, Q. Allometry-Based Estimation of Forest Aboveground Biomass Combining LiDAR Canopy Height Attributes and Optical Spectral Indexes. *For. Ecosyst.* **2022**, *9*, 100059. [CrossRef]
8. Qin, H.; Zhou, W.; Yao, Y.; Wang, W. Estimating Aboveground Carbon Stock at the Scale of Individual Trees in Subtropical Forests Using UAV LiDAR and Hyperspectral Data. *Remote Sens.* **2021**, *13*, 4969. [CrossRef]
9. López-Serrano, P.; López Sánchez, C.; Solís-Moreno, R.; Corral-Rivas, J. Geospatial Estimation of above Ground Forest Biomass in the Sierra Madre Occidental in the State of Durango, Mexico. *Forests* **2016**, *7*, 70. [CrossRef]
10. Domingo, D.; Ørka, H.O.; Næsset, E.; Kachamba, D.; Gobakken, T. Effects of UAV Image Resolution, Camera Type, and Image Overlap on Accuracy of Biomass Predictions in a Tropical Woodland. *Remote Sens.* **2019**, *11*, 948. [CrossRef]
11. Zhu, Y.; Liu, K.; Myint, S.W.; Du, Z.; Li, Y.; Cao, J.; Liu, L.; Wu, Z. Integration of GF2 Optical, GF3 SAR, and UAV Data for Estimating Aboveground Biomass of China's Largest Artificially Planted Mangroves. *Remote Sens.* **2020**, *12*, 2039. [CrossRef]
12. Luo, S.; Wang, C.; Xi, X.; Pan, F.; Peng, D.; Zou, J.; Nie, S.; Qin, H. Fusion of Airborne LiDAR Data and Hyperspectral Imagery for Aboveground and Belowground Forest Biomass Estimation. *Ecol. Indic.* **2017**, *73*, 378–387. [CrossRef]
13. Liang, X.; Kankare, V.; Hyyppä, J.; Wang, Y.; Kukko, A.; Haggrén, H.; Yu, X.; Kaartinen, H.; Jaakkola, A.; Guan, F.; et al. Terrestrial Laser Scanning in Forest Inventories. *ISPRS J. Photogramm. Remote Sens.* **2016**, *115*, 63–77. [CrossRef]
14. Jin, S.; Sun, X.; Wu, F.; Su, Y.; Li, Y.; Song, S.; Xu, K.; Ma, Q.; Baret, F.; Jiang, D.; et al. LiDAR Sheds New Light on Plant Phenomics for Plant Breeding and Management: Recent Advances and Future Prospects. *ISPRS J. Photogramm. Remote Sens.* **2021**, *171*, 202–223. [CrossRef]
15. Lu, J.; Wang, H.; Qin, S.; Cao, L.; Pu, R.; Li, G.; Sun, J. Estimation of Aboveground Biomass of Robinia Pseudoacacia Forest in the Yellow River Delta Based on UAV and Backpack LiDAR Point Clouds. *Int. J. Appl. Earth Obs. Geoinfor.* **2020**, *86*, 102014. [CrossRef]
16. Chen, C.C.; Liu, Q.W.; Li, C.; Li, M.; Zhou, X.; Yu, C.; Su, K. Comparison of linear and nonlinear models for carbon stock estimation in plantation forests based on UAV LiDAR. *J. Beijing For. Univ.* **2021**, *43*, 9–16.
17. Luo, S.; Wang, C.; Xi, X.; Nie, S.; Fan, X.; Chen, H.; Ma, D.; Liu, J.; Zou, J.; Lin, Y.; et al. Estimating Forest Aboveground Biomass Using Small-Footprint Full-Waveform Airborne LiDAR Data. *Int. J. Appl. Earth Obs. Geoinfor.* **2019**, *83*, 101922. [CrossRef]
18. Cao, L.; Pan, J.; Li, R.; Li, J.; Li, Z. Integrating Airborne LiDAR and Optical Data to Estimate Forest Aboveground Biomass in Arid and Semi-Arid Regions of China. *Remote Sens.* **2018**, *10*, 532. [CrossRef]
19. Su, Y.; Guo, Q.; Fry, D.L.; Collins, B.M.; Kelly, M.; Flanagan, J.P.; Battles, J.J. A Vegetation Mapping Strategy for Conifer Forests by Combining Airborne LiDAR Data and Aerial Imagery. *Can. J. Remote Sens.* **2016**, *42*, 1–15. [CrossRef]
20. Li, W.; Niu, Z.; Chen, H.; Li, D.; Wu, M.; Zhao, W. Remote Estimation of Canopy Height and Aboveground Biomass of Maize Using High-Resolution Stereo Images from a Low-Cost Unmanned Aerial Vehicle System. *Ecol. Indic.* **2016**, *67*, 637–648. [CrossRef]
21. Li, Q.; Wong, F.K.K.; Fung, T. Mapping Multi-Layered Mangroves from Multispectral, Hyperspectral, and LiDAR Data. *Remote Sens. Environ.* **2021**, *258*, 112403. [CrossRef]
22. Popescu, S.; Wynne, R.; Scrivani, J. Fusion of Small-Footprint LiDAR and Multispectral Data to Estimate Plot- Level Volume and Biomass in Deciduous and Pine Forests in Virginia, USA. *For. Sci.* **2004**, *50*, 551–565.
23. Brown, S.; Narine, L.L.; Gilbert, J. Using Airborne LiDAR, Multispectral Imagery, and Field Inventory Data to Estimate Basal Area, Volume, and Aboveground Biomass in Heterogeneous Mixed Species Forests: A Case Study in Southern Alabama. *Remote Sens.* **2022**, *14*, 2708. [CrossRef]
24. Kim, S.-R.; Kwak, D.-A.; oLee, W.-K.; Son, Y.; Bae, S.-W.; Kim, C.; Yoo, S. Estimation of Carbon Storage Based on Individual Tree Detection in Pinus Densiflora Stands Using a Fusion of Aerial Photography and LiDAR Data. *Sci. China Life Sci.* **2010**, *53*, 885–897. [CrossRef] [PubMed]
25. Yang, H.; Hu, C.M.; Zhang, L.M.; Li, S.G. Progress in the characterization of forest carbon sinks in Inner Mongolia. *J. Appl. Ecol.* **2014**, *25*, 3366–3372. [CrossRef]
26. Fang, C.L.; Chen, Q.; Ren, C.; Wang, Y.J. Airborne LiDAR-based modeling of subtropical forest biomass estimation. *For. Surv. Plan.* **2021**, *46*, 1–8.
27. Han, M.C. Exploration of biomass and productivity of Xing'an larch plantation. *J. North China Agric.* **1987**, *5*, 134–138.

28. Abbas, F.; Hammad, H.M.; Fahad, S.; Cerdà, A.; Rizwan, M.; Farhad, W.; Ehsan, S.; Bakhat, H.F. Agroforestry: A Sustainable Environmental Practice for Carbon Sequestration under the Climate Change Scenarios—A Review. *Environ. Sci. Pollut. Res.* **2017**, *24*, 11177–11191. [CrossRef]

29. Rouse, J.W., Jr.; Haas, R.H.; Schell, J.A.; Deering, D.W. Monitoring Vegetation Systems in the Great Plains with Erts. *NASA Spec. Publ.* **1974**, *351*, 309.

30. Pearson, R.L.; Miller, L.D. Remote Mapping of Standing Crop Biomass for Estimation of the Productivity of the Shortgrass Prairie. *Remote Sens. Environ.* **1972**, *VIII*, 1355. [CrossRef]

31. Miura, T.; Yoshioka, H.; Fujiwara, K.; Yamamoto, H. Inter-Comparison of ASTER and MODIS Surface Reflectance and Vegetation Index Products for Synergistic Applications to Natural Resource Monitoring. *Sensors* **2008**, *8*, 2480–2499. [CrossRef]

32. Jordan, C.F. Derivation of Leaf-Area Index from Quality of Light on the Forest Floor. *Ecology* **1969**, *50*, 663–666. [CrossRef]

33. Huete, A.R. A Soil-Adjusted Vegetation Index (SAVI). *Remote Sens. Environ.* **1988**, *25*, 295–309. [CrossRef]

34. Han, A.H. Research on Remote Sensing Methods for Monitoring Forest Biomass and Carbon Stock. Ph.D. Thesis, Beijing Forestry University, Beijing, China, 2009; 146p.

35. Lu, L.; Zheng, G.; Ma, L. Estimation of effective leaf area index of forest by combining LiDAR and point cloud slicing algorithm. *J. Remote Sens.* **2018**, *22*, 432–449.

36. Hyyppä, E.; Yu, X.; Kaartinen, H.; Hakala, T.; Kukko, A.; Vastaranta, M.; Hyyppä, J. Comparison of Backpack, Handheld, Under-Canopy UAV, and Above-Canopy UAV Laser Scanning for Field Reference Data Collection in Boreal Forests. *Remote Sens.* **2020**, *12*, 3327. [CrossRef]

37. Ruhan, A.; Du, W.; Ying, H.; Wei, B.; Shan, Y.; Dai, H. Estimation of Aboveground Biomass of Individual Trees by Backpack LiDAR Based on Parameter-Optimized Quantitative Structural Models (AdQSM). *Forests* **2023**, *14*, 475. [CrossRef]

38. Jiao, Y.; Wang, D.; Yao, X.; Wang, S.; Chi, T.; Meng, Y. Forest Emissions Reduction Assessment Using Optical Satellite Imagery and Space LiDAR Fusion for Carbon Stock Estimation. *Remote Sens.* **2023**, *15*, 1410. [CrossRef]

39. Wang, C.; Feng, M.-C.; Yang, W.-D.; Ding, G.-W.; Sun, H.; Liang, Z.-Y.; Xie, Y.-K.; Qiao, X.-X. Impact of Spectral Saturation on Leaf Area Index and Aboveground Biomass Estimation of Winter Wheat. *Spectrosc. Lett.* **2016**, *49*, 241–248. [CrossRef]

40. Campbell, M.J.; Dennison, P.E.; Kerr, K.L.; Brewer, S.C.; Anderegg, W.R.L. Scaled Biomass Estimation in Woodland Ecosystems: Testing the Individual and Combined Capacities of Satellite Multispectral and LiDAR Data. *Remote Sens. Environ.* **2021**, *262*, 112511. [CrossRef]

41. Jiang, F.; Deng, M.; Tang, J.; Fu, L.; Sun, H. Integrating Spaceborne LiDAR and Sentinel-2 Images to Estimate Forest Aboveground Biomass in Northern China. *Carbon Balance Manag.* **2022**, *17*, 1–13. [CrossRef]

42. Guerra-Hernández, J.; Narine, L.L.; Pascual, A.; Gonzalez-Ferreiro, E.; Botequim, B.; Malambo, L.; Neuenschwander, A.; Popescu, S.C.; Godinho, S. Aboveground Biomass Mapping by Integrating ICESat-2, SENTINEL-1, SENTINEL-2, ALOS2/PALSAR2, and Topographic Information in Mediterranean Forests. *GIScience Remote Sens.* **2022**, *59*, 1509–1533. [CrossRef]

43. Huang, H.; Liu, C.; Wang, X.; Zhou, X.; Gong, P. Integration of Multi-Resource Remotely Sensed Data and Allometric Models for Forest Aboveground Biomass Estimation in China. *Remote Sens. Environ.* **2019**, *221*, 225–234. [CrossRef]

44. Shen, W.; Li, M.; Huang, C.; Tao, X.; Wei, A. Annual Forest Aboveground Biomass Changes Mapped Using ICESat/GLAS Measurements, Historical Inventory Data, and Time-Series Optical and Radar Imagery for Guangdong Province, China. *Agric. For. Meteorol.* **2018**, *259*, 23–38. [CrossRef]

45. Coops, N.C.; Tompalski, P.; Goodbody, T.R.H.; Queinnec, M.; Luther, J.E.; Bolton, D.K.; White, J.C.; Wulder, M.A.; van Lier, O.R.; Hermosilla, T. Modelling LiDAR-Derived Estimates of Forest Attributes over Space and Time: A Review of Approaches and Future Trends. *Remote Sens. Environ.* **2021**, *260*, 112477. [CrossRef]

46. Schlund, M.; Scipal, K.; Quegan, S. Assessment of a Power Law Relationship Between P-Band SAR Backscatter and Aboveground Biomass and Its Implications for BIOMASS Mission Performance. *IEEE J. Sel. Top. Appl. Earth Obs. Remote Sens.* **2018**, *11*, 3538–3547. [CrossRef]

47. Sadadi, O.; Hussin, Y.A.; Kloosterman, H.; Ismail, M.H. Tropical rain forest tree height measurement using ALS and TLS for estimating forest biomass and carbon stock in Ayer Hitam Forest, Malaysia. In Proceedings of the Asian Conference on Remote Sensing ACRS, Colombo, Sri Lanka, 17–21 October 2016; Volume 10, pp. 925–934.

48. Silva, C.A.; Klauberg, C.; Hudak, A.T.; Vierling, L.A.; Fennema, S.J.; Corte, A.P.D. Modeling and Mapping Basal Area of Pinus Taeda, L. Plantation Using Airborne LiDAR Data. *An. Acad. Bras. Ciênc.* **2017**, *89*, 1895–1905. [CrossRef]

49. Sheridan, R.D.; Popescu, S.C.; Gatziolis, D.; Morgan, C.L.S.; Ku, N.-W. Modeling Forest Aboveground Biomass and Volume Using Airborne LiDAR Metrics and Forest Inventory and Analysis Data in the Pacific Northwest. *Remote Sens.* **2015**, *7*, 229–255. [CrossRef]